Strike-slip fault terminations at seismogenic depths: The structure and kinematics of the Glacier Lakes fault, Sierra Nevada United States

J. D. Kirkpatrick,[1] Z. K. Shipton,[1] J. P. Evans,[2] S. Micklethwaite,[3] S. J. Lim,[2] and P. McKillop[2,4]

[1] Structural complexity is common at the terminations of earthquake surface ruptures; similar deformation may therefore be expected at the end zones of earthquake ruptures at depth. The 8.2 km long Glacier Lakes fault (GLF) in the Sierra Nevada is a left-lateral strike-slip fault with a maximum observed displacement of 125 m. Within the fault, pseudotachylytes crosscut cataclasites, showing that displacement on the GLF was accommodated at least partly by seismic slip. The western termination of the GLF is defined by a gradual decrease in the displacement on the main fault, accompanied by a 1.4 km wide zone of secondary faulting in the dilational quadrant of the GLF. The secondary faults splay counterclockwise from the main fault trace forming average angles of 39° with the main fault. Slip vectors defined by slickenlines plunge more steeply west for these splay faults than for the GLF. Static stress transfer modeling shows that the orientations of the splays, and the plunge of displacement on those splays, are consistent with displacement on the main fault. The GLF termination structure shows that structural complexity is present at the terminations of faults at seismogenic depths and therefore ruptures that propagate beyond fault terminations, or through step overs between two faults, will likely interact with complex secondary fault structures. Models of dynamic rupture propagation must account for the effect of preexisting structures on the elastic properties of the host rock. Additionally, aftershock distributions and focal mechanisms may be controlled by the geometry and kinematics of structures present at fault terminations.

1. Introduction

[2] Fault terminations are the transition from well-developed slip surfaces to unbroken host or country rock ahead of the fault tip. Commonly, the ends of faults are associated with zones of structural complexity that encompass both macroscale and microscale deformation elements [*McGrath and Davison*, 1995; *Vermilye and Scholz*, 1998; *Shipton and Cowie*, 2001; *Storti et al.*, 2001; *Pachell and Evans*, 2002; *Kim and Sanderson*, 2006]. Fault terminations are also associated with regions of enhanced mineralization implying greater permeability for hydrothermal fluid migration is produced during deformation in these regions, which may be directly related to earthquake and aftershock behavior [*Sibson*, 1985, 1987; *Curewitz and Karson*, 1997; *Micklethwaite and Cox*, 2004, 2006].

[3] Observations of surface ruptures associated with strike-slip faults show that the majority of earthquakes end at geometric complexities, including fault terminations [*King and Nabelek*, 1985; *DePolo et al.*, 1991; *Wesnousky*, 2006]. The physical properties of fault terminations therefore control to some extent the size of earthquake ruptures [e.g., *Aki*, 1979; *Segall and Pollard*, 1980; *Sibson*, 1989]. Rupture propagation is also observed to decelerate in regions of structural complexity, suggesting interdependence between fault properties and earthquake processes [*Aydin and Du*, 1995; *Barka*, 1996; *Andrews*, 2005]. Three-dimensional numerical modeling has shown that structural discontinuities can act as barriers to earthquake propagation in some cases, but allow ruptures to propagate through in other cases [e.g., *Harris and Day*, 1999], and highlights the significance of the edges of faults to both earthquake propagation and termination [*Kase and Kuge*, 2001]. Understanding the geometry and kinematics of fault termination structures is therefore important for interpreting the processes by which earthquakes stop.

[1]Department of Geographical and Earth Sciences, University of Glasgow, Glasgow, UK.
[2]Department of Geology, Utah State University, Logan, Utah, USA.
[3]Research School of Earth Sciences, Australian National University, Canberra ACT, Australia.
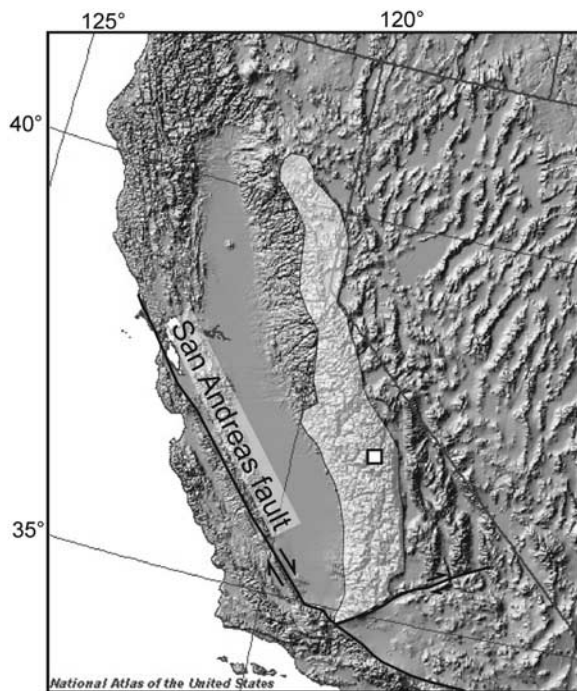[4]Deceased 1999.

Figure 1. Shaded elevation map of California and western margin of North America showing location of study area (white box). Shaded area indicates the extent of the Sierra Nevada granitic plutons. Base map is from the National Atlas of the United States (http://nationalatlas.gov).

[4] Field studies of geologic structures exhumed from seismogenic depths help address some of the current questions in earthquake seismology regarding earthquake rupture processes, such as the following:

[5] 1. Are the zones of structural complexity that are associated with the terminations of faults at the Earth's surface also present at depth in the crust?

[6] 2. What processes are responsible for the generation of off-fault damage observed at the terminations of many faults?

[7] 3. Are the physical properties of fault terminations different to the properties of well-developed faults far from segment ends, and how could this influence earthquake rupture processes?

[8] 4. Are aftershock distributions controlled to some extent by the geometry of the structures associated with fault terminations?

[9] We explore these questions by examining field exposures of faults that formed at depths equivalent to those where earthquakes are observed to nucleate. Exhumation of the Sierra Nevada batholith, California, has resulted in large along-strike exposures of faults that are inferred to have been active at depths of ~6–8 km [*Ague and Brimhall*, 1988]. The faults are pseudotachylyte-bearing and so experienced slip events that occurred at seismic velocities [*Cowan*, 1999]. The pseudotachylytes are not the focus of this paper, but the presence of cooled friction-induced melts in the faults means that the field data presented in this study are directly relevant to the investigation of earthquake rupture processes.

[10] We present structural and kinematic data from the western termination of the Glacier Lakes fault (GLF), a left-lateral strike-slip fault with a minimum length of 8.2 km and a maximum observed strike separation of about 125 m [*Evans et al.*, 2000]. The fault cuts relatively homogeneous granites and granodiorites that have been exhumed without significant associated deformation. Field observations provide detail of fault geometry, composition and inferred deformation processes beyond that which may be collected utilizing only geophysical techniques or deep drilling. Assuming that the entire observed length of this fault had slipped in a single event, it would have produced an earthquake of magnitude 5.7 or greater (using scaling relations from *Wells and Coppersmith* [1994]). A structure of this scale is likely the size of fault that would break to, or near to, the Earth's surface and would have ruptured most of the thickness of the brittle crust. Using static stress transfer modeling we show that the structures found at the termination of the GLF are consistent with earthquake slip on the main structure. We compare our data with the characteristics of termination structures observed for other faults, and discuss the implications for the termination of earthquake ruptures.

2. Geologic Setting

[11] The study area is located in the northern part of Sequoia and Kings Canyon National Park, Sierra Nevada, California (Figure 1). Excellent exposures exist due to recent glaciation and climate at altitudes greater than 3000 m, with vertical relief in the study area of ~500 m. The Sierra Nevada is dominated by Mesozoic granite and granodiorite plutons that represent the remains of a continental magmatic arc which stretches along the west coast of North America [*Moore*, 1978; *Bateman*, 1992]. Metamorphosed sedimentary and volcaniclastic roof pendants are also present, preserved in narrow seams between plutons [*Moore*, 1978]. Pluton boundaries and late stage aplite dikes can be used as markers to determine the magnitude of displacement on the faults.

[12] Published K-Ar ages of biotites from two of the plutons in the study area represent the time before present at which the minerals last passed below 300°C, the closure temperature of biotite with respect to argon [*Berger and York*, 1981]. Biotites from the Cartridge Pass granodiorite cooled at 81 ± 3 Ma [*Dodge and Moore*, 1968], and the LeConte Canyon alaskite biotites cooled at 80 ± 0.24 Ma [*Evernden and Kistler*, 1970]. These ages are interpreted to represent the crystallization ages of the biotites during the emplacement of the two plutons respectively. None of the plutons cut by the GLF have been dated. However, as the Cartridge Pass and LeConte Canyon plutons are among the youngest in the study area, the relative ages of the rocks cut by the GLF are inferred to be lower-mid-Cretaceous [*Moore*, 1978]. Aluminum-in-hornblende palaeogeobarometry estimates indicate the depth of crystallization of the central Sierra Nevada plutons is mostly 8–11 km, but is as little as 4 km in some cases [*Noyes et al.*, 1983; *Ague and Brimhall*, 1988]. Plutons in this area were most likely emplaced by passive intrusion into tectonically controlled tensile regions based on the existence of joints [*Tobisch and*
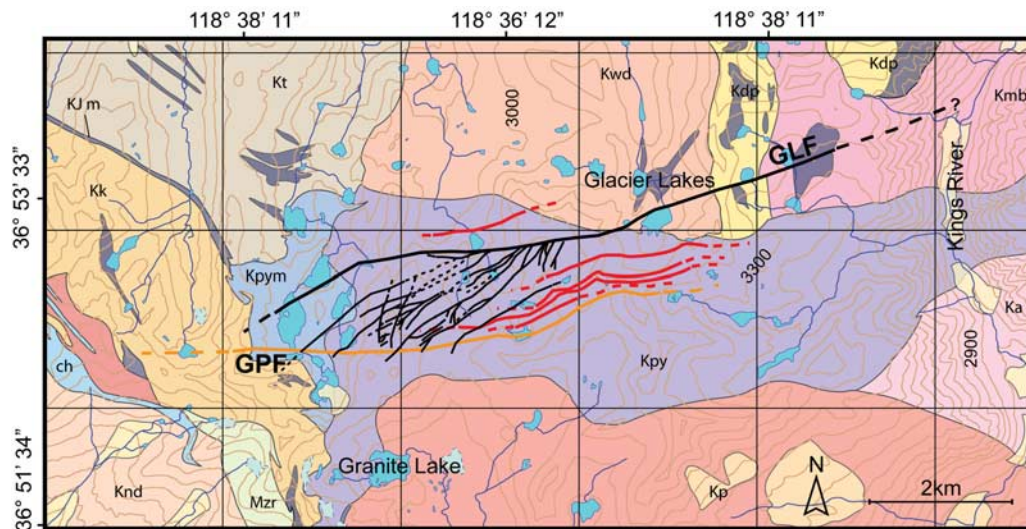
Figure 2. Map showing overall geometry of structures present in study area as determined by air photo interpretation and field observations (GLF is Glacier Lakes Fault, black faults are associated splays, GPF is Granite Pass Fault, red faults are faults subparallel to the GPF, contours are at 50 m intervals; faults are dashed where uncertain). Plutons are outlined in different colors [after *Moore*, 1978]: Kpy; Pyramid pluton, Kk; Kennedy Lakes pluton (for clarity, not all individual plutons are named).

Cruden, 1995], and the existence of a synmagmatic shear zone [*Tikoff and de Saint Blanquat*, 1997].

[13] Many of the left-lateral strike-slip faults in the central Sierra Nevada nucleated on preexisting joints that formed in response to pluton cooling [*Segall and Pollard*, 1983]. Slip on reactivated joints increased stress at the tips of small faults, which in some cases resulted in the formation of oblique secondary fractures, termed splay fractures [*Segall and Pollard*, 1980; *Martel and Boger*, 1998; *Martel et al.*, 1988]. These opening mode fractures link noncoplanar faults across discontinuities defined as steps (parallel faults) and bends (nonparallel faults). Continued linkage through splay fracture generation leads to the development of 'simple fault zones' characterized by two subparallel faults bounding a tabular volume of fractured host rock [*Martel et al.*, 1988]. Simple fault zones may be up to a kilometer in length and accommodate as much as 10 m displacement. 'Compound fault zones' represent the final stage of fault evolution described by *Martel* [1990] for the Sierra Nevada and are up to several kilometers long, accommodating displacements as great as 100 m. In other areas faults have also nucleated on preexisting dikes weakened by closely spaced joints [*Christiansen and Pollard*, 1997; *d'Alessio and Martel*, 2005].

[14] Geological evidence strongly suggests that the studied faults were active in the seismogenic zone. K-Ar and Ar-Ar dating of muscovite from similar faults located in the Mount Abbot Quadrangle, ∼55 km to the north of the study area, estimate the age of formation of those faults to be 79.7 ± 0.16 Ma [*Pachell and Evans*, 2002] and 78.9 ± 0.4 Ma [*Segall et al.*, 1990]. Reported K-Ar crystallization ages of biotites in the host rock to the faults of 82 Ma and 77 Ma [*Evernden and Kistler*, 1970] indicate that the Mount Abbot faults were active soon after pluton emplacement. The faults in the Mount Abbot Quadrangle also display both brittle and ductile deformation fabrics, suggesting that they were active

toward the base of the seismogenic zone [*Christiansen and Pollard*, 1997]. If the GLF also formed soon after pluton emplacement, the amount of erosion since pluton crystallization in the study area suggests the fault would have been active at around 6–8 km depth [*Ague and Brimhall*, 1988; *House et al.*, 1998].

3. Field Observations

[15] The study area contains two large fault zones; the Glacier Lakes fault (GLF), and the older Granite Pass fault (GPF), as well as several smaller faults that are subparallel to the GPF (Figure 2). In this paper we focus on the western termination of the GLF which is characterized by a set of smaller faults that splay in a counterclockwise sense from the GLF. The geometry of the structures in the area has been defined using a combination of air photo interpretation and field mapping. Total displacement at a given point is calculated by using offset pluton boundaries and aplite dikes. Where exposed, the intersection of two dikes was used to define a piercing point to directly measure the total displacement. Offset pluton boundaries and single dikes could also be used to define the displacement where slip vectors were measured from slickenlines on exposed slip surfaces.

3.1. Granite Pass Fault

[16] The GPF is a relatively shallowly dipping (40–70°S) left-lateral strike-slip fault that trends approximately ENE (Figure 3). The mapped extent of the GPF shows that it has a minimum trace length of 6.7 km, and a maximum observed displacement of ∼80 m. Fault thickness, measured orthogonal to the fault plane, is highly variable along strike but is typically on the scale of tens of meters. The fault can be traced by aligned outcrops containing gray-green to black colored deformed rocks (Figure 4a). Mylonitic tex-
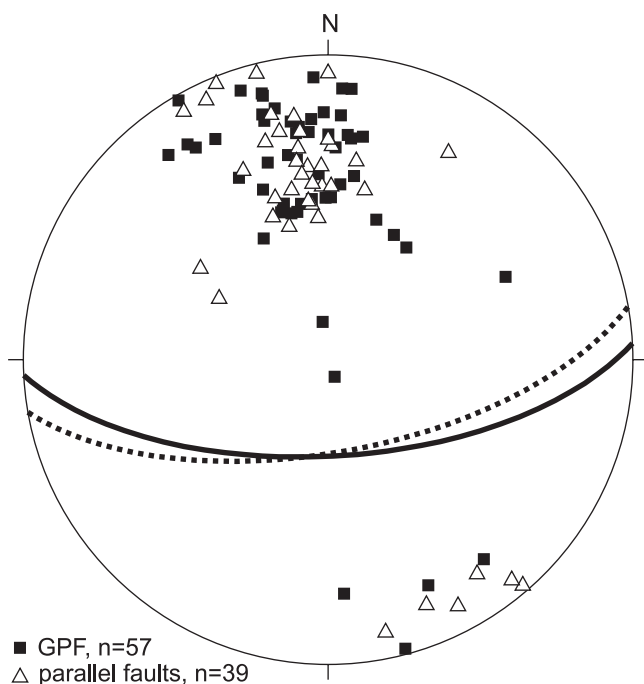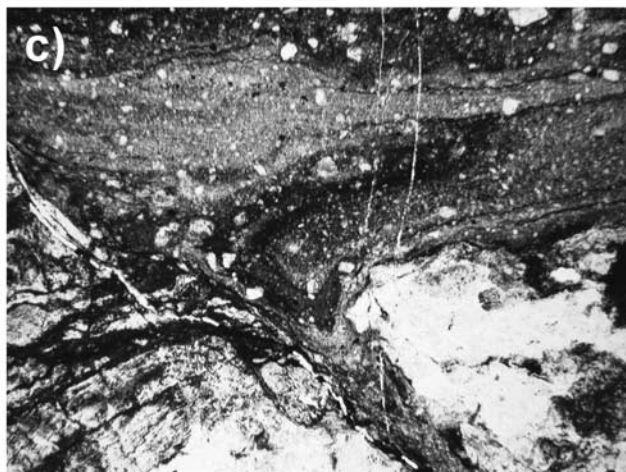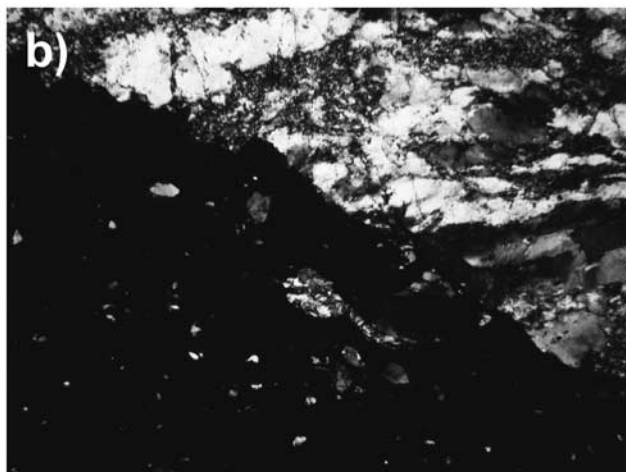
Figure 3. Structural analysis of the GPF and subparallel faults (equal-area projection). Stereonet shows poles to GPF fault plane orientations (filled squares), poles to subparallel fault orientations (open triangles), and two great circles representing the average orientation of the GPF (solid line) and subparallel faults (dotted line).

tures that develop at high temperatures and/or pressures are present in the GPF indicating that the fault started to form soon after the pluton was emplaced at depth. These deformation textures, combined with crosscutting relations (see below) indicate that the GPF is the oldest structure present in the study area.

[17] The GPF is characterized by a heterogeneous strain distribution across a wide zone of deformed rock. Up to three fault core strands may be present, ranging in thickness from centimeters to meters, which are observed to bifurcate and anastomose along strike. Deformation elements within the fault core strands include cataclasites and ultracataclasites that overprint ductile fabrics developed in the wall rock. Cataclasites are present in seams millimeters to centimeters thick and range from slightly fractured host rock to cohesive fault gouge that has undergone extensive

Figure 4. (a) An outcrop of the GPF containing dark colored deformed rock. Clipboard is 33 cm long. (b) Photomicrograph (crossed polars) of ultracataclasite from the GPF showing ultrafine-grained groundmass and clasts of varying composition. Note the recrystallized quartz in the wall rock, showing that early ductile deformation is overprinted by later cataclastic deformation. (c) Photomicrograph (plain polarized light) of pseudotachylyte from the GPF. Main vein runs left to right with an injection vein branching off at high angle toward the bottom right of the image. Flow fabrics and embayed clasts within the pseudotachylyte indicate a melt origin for these rocks. Field of view in both micrographs is 3.1 mm.
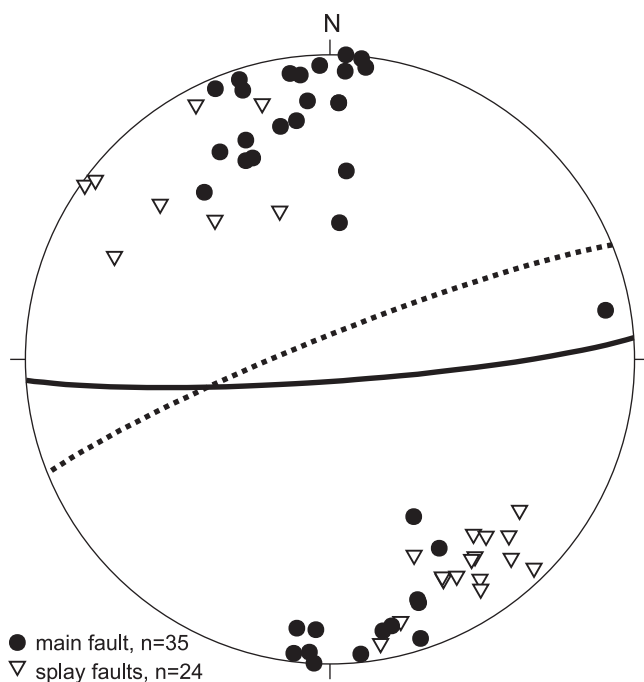
Figure 5. Structural analysis of the GLF and splay faults (equal-area projection). Poles to measured GLF orientations (filled circles) and poles to splay fault orientations (open triangles) are shown with great circles representing the average orientation of the GLF (solid line) and splay faults (dotted line).

grain size reduction and comminution. Cataclastic shear fabrics are rarely evident in outcrop, but are present in thin section and show crosscutting relations consistent with left-lateral displacement. Ultracataclasites range in thickness from centimeters to meters, are very dark, aphanitic, and demonstrate faint flow-like fabrics in hand specimen. Clasts present within the ultracataclasites are ≤0.5 mm, rounded and are composed of quartz, feldspar and multicrystal fragments of wall rock (Figure 4b). Subsidiary opening mode and shear fractures are ubiquitous throughout the fault zone, are closely spaced and are present both between and outside of the fault core strands.

[18] Slip surfaces can be identified from slickenlines on exposed fracture surfaces, and by pseudotachylyte generation surfaces. Slip surfaces are exposed as polished rock faces upon which aligned elongate chlorite and epidote minerals are present defining slickenlines. The surfaces are typically corrugated (with millimeters to centimeters amplitude) in the direction parallel to slickenlines, and are often found at the edges of, or overprinting, fault core strands as well as between strands. Pseudotachylyte generation surfaces are present as thin (≤10 mm), approximately planar veins with associated high angle injection veins distributed throughout the fault. In hand specimen, pseudotachylyte material is dark gray to black, and often shows banded coloration. Veins have sharp edges with the wall rock, regardless of whether they overprint undeformed host rock, cataclasite or ultracataclasite. Flow fabrics and spherulitic textures developed in the veins (Figure 4c) provide evidence for a melt origin for these fault rocks.

[19] A series of faults that are subparallel to the GPF are also present in the study area (Figures 2 and 3). These faults all have mapped trace lengths of 1–4 km, with displacements of tens of meters and display similar deformation features to the GPF. One or more fault core strands are present within each fault zone. The fault cores contain cataclasites, ultracataclasites, mylonites and occasional pseudotachylytes. Fault core strands vary in thickness from tens of centimeters to several meters, with thickness varying by an order of magnitude within tens meters along strike. Fault zone widths defined by the fault core and damage zones for the faults range from around a meter to tens of meters. The similarity in the orientation and architecture of these faults with the GPF suggests that they share a common deformation history. The GPF-parallel faults also consistently display the same crosscutting relations as the GPF, and so are inferred to be older than the GLF and splay faults.

3.2. Glacier Lakes Fault

[20] The ENE trending GLF dips 70–90°S (Figure 5) and has been mapped for 8.2 km along strike with a maximum observed left lateral strike separation of ∼125 m. The eastern termination of the fault has not been directly observed and so the total length of the fault remains uncertain. However, air photo analysis indicates the fault continues along strike at least to the King's River canyon implying that 8.2 km is a minimum estimate of the total fault length (see Figure 2). The fault zone is characterized by two subparallel, approximately planar faults encompassing a region of highly fractured host rock. Subsidiary fractures form at high angles to the bounding faults to the GLF, and are often associated with alteration of the host rock by fluid flow. Such structures are rarely present outside the bounding faults, and are generally short (lengths less than several meters) where observed. The fractured rock between bounding faults is often preferentially eroded causing the fault to be expressed as a topographic trough up to 60 m wide, representing the width of the fault zone (Figure 6a). Mylonitic fabrics indicative of ductile regime deformation are generally absent from the fault zone.

[21] The bounding faults within the GLF are up to several centimeters thick and contain gray-green foliated cataclasites composed of comminuted host rock fragments as well as abundant epidote and chlorite that are the products of fluid-related mineralization. Thin section analysis of the bounding faults shows that the cataclasites are texturally complex, comprising domains of deformed rock with different properties (Figure 6b). Domains are generally separated from one another by slip surfaces and vary from cataclasites comprising ultrafine-grained, epidote-rich matrix (90%) with rounded clasts (10%) ≤0.2 mm in diameter, to cataclasites comprising predominantly subrounded clasts (85%) ≤1 mm in diameter. In thin section it can be observed that pseudotachylyte is present in veins of variable thickness crosscutting the cataclasites in the bounding faults. Pseudotachylyte veins contain microcrystallites (Figure 6c), and spherulitic textures. Extensive chlorite developed in the groundmass indicates that the pseudotachylyte has undergone some degree of alteration subsequent to crystallization.

[22] Distinct slickenlines defined by the aligned long axes of chlorite and epidote minerals, as well as grooves and
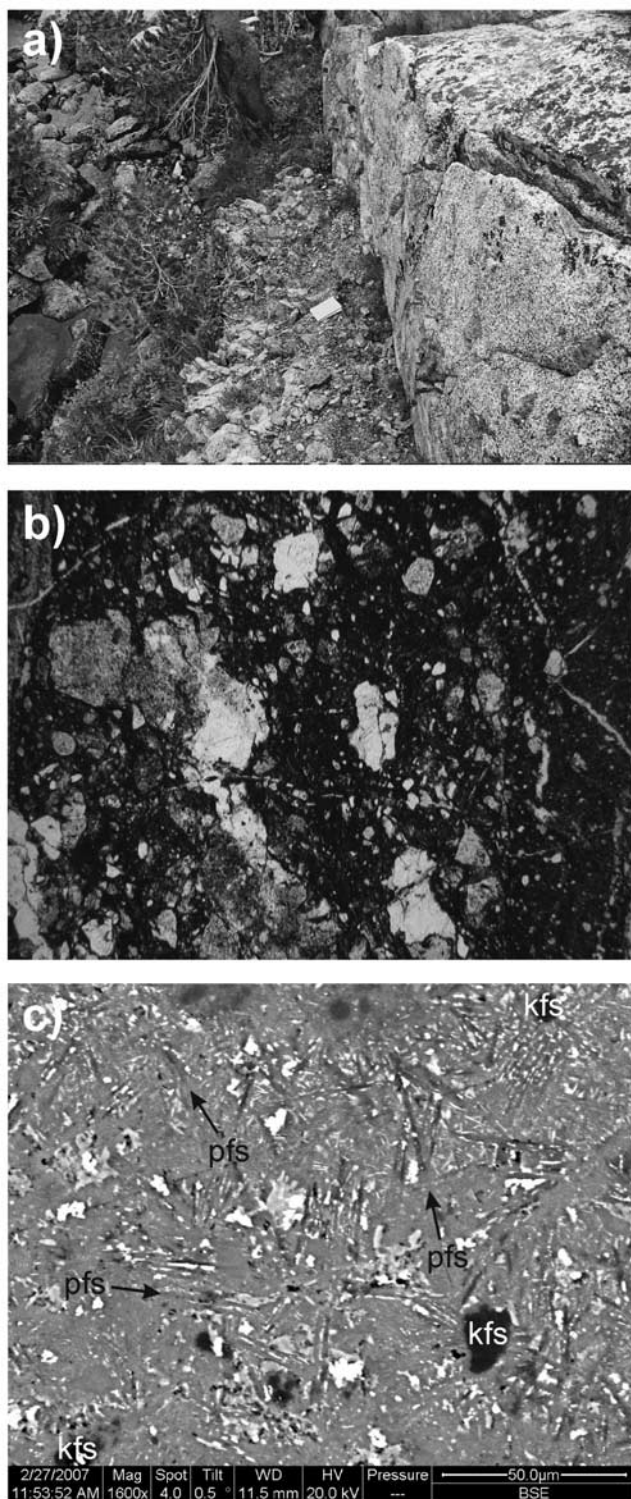
Figure 6. (a) Typical outcrop of the GLF topographic trough bounded by fault planes (notebook is 20 cm long). (b) Photomicrograph (plane polarized light) of cataclasite from the bounding fault to the GLF showing angular clasts and fabric domains with differing clast size and clast to matrix ratios. Field of view is 3 mm. (c) Backscatter electron microscope image of pseudotachylyte from the GLF showing plagioclase microcrystallites (pfs) and clasts of K-feldspar (kfs).

corrugations, occur on slip surfaces on the bounding faults. Slickenline orientations on slip surfaces indicate predominantly strike-slip displacement, with the majority (74%) of measured orientations raking $\leq 30°$ from the horizontal (Figure 7a). The most oblique rakes observed (up to 76°) have no obvious systematic spatial variation, and do not seem to correlate with macroscale fault geometry. A similar number of slickenlines rake east (38%) as rake west (53%). The plunge of the slickenlines does not indicate the relative sense of displacement, but because markers are consistently offset left-laterally, these data can be used in combination to determine the net displacement.

3.3. GLF Termination

[23] The GLF terminates at its western end in a series of smaller faults that splay counterclockwise from the main trace of the GLF in a northeast-southwest orientation. The splay faults are up to 3 km long and form a zone of secondary faulting ~1.4 km wide that is restricted to the termination region. Splay faults form dihedral angles with the GLF ranging from 13 to 60°, with a mean of 39° (see Figure 5). These splay faults are in the dilational quadrant for the left lateral GLF. The compressional quadrant to the north of the GLF does not exhibit any macroscale deformation structures.

[24] The splay faults are defined by topographic troughs up to 13 m wide. These fault troughs are bounded by slip surfaces decorated with dark green to black chlorite and epidote mineralization. Cataclasite seams with a maximum thickness of ~1 cm are occasionally preserved at the edges of the fault troughs. The similarities between the expression of the splay faults and the GLF suggest that the splay faults have deformed by similar deformation mechanisms to the GLF.

[25] All of the splay faults cut and displace dikes with a left-lateral to oblique sense of displacement. In five places, the splay faults are observed to crosscut and displace the GPF, indicating that the GPF is an older structure. Rake magnitudes recorded along strike for one of the splay fault sets (S2 and associated splay W1) show a maximum rake of 58°, with 77% of slickenlines raking between 20 to 40° to the southwest (Figure 7b). The sense of displacement for the splay faults is therefore more oblique than for the GLF.

[26] The cumulative displacement distribution along the splay faults has been calculated from dike offset and from the rakes of slickenlines (Figure 8). Displacement on the GLF decreases toward zero in the west where the boundary between the Pyramid and adjacent Kennedy Lakes plutons is not offset, marking the termination of the fault. Displacement profiles for the splay faults are constructed from a limited data set as there are few dikes offset by the fault that can be used as displacement indicators. However, it is apparent that displacement on the splay faults is generally greatest close to the GLF and decreases to the southwest. Two of the splays (S2 and S3) show displacement maxima located away from the main fault, with displacement subsequently decreasing as the GLF is approached.

4. Interpretation

[27] The western termination of the GLF is defined by a gradual decrease in the displacement on the main fault zone
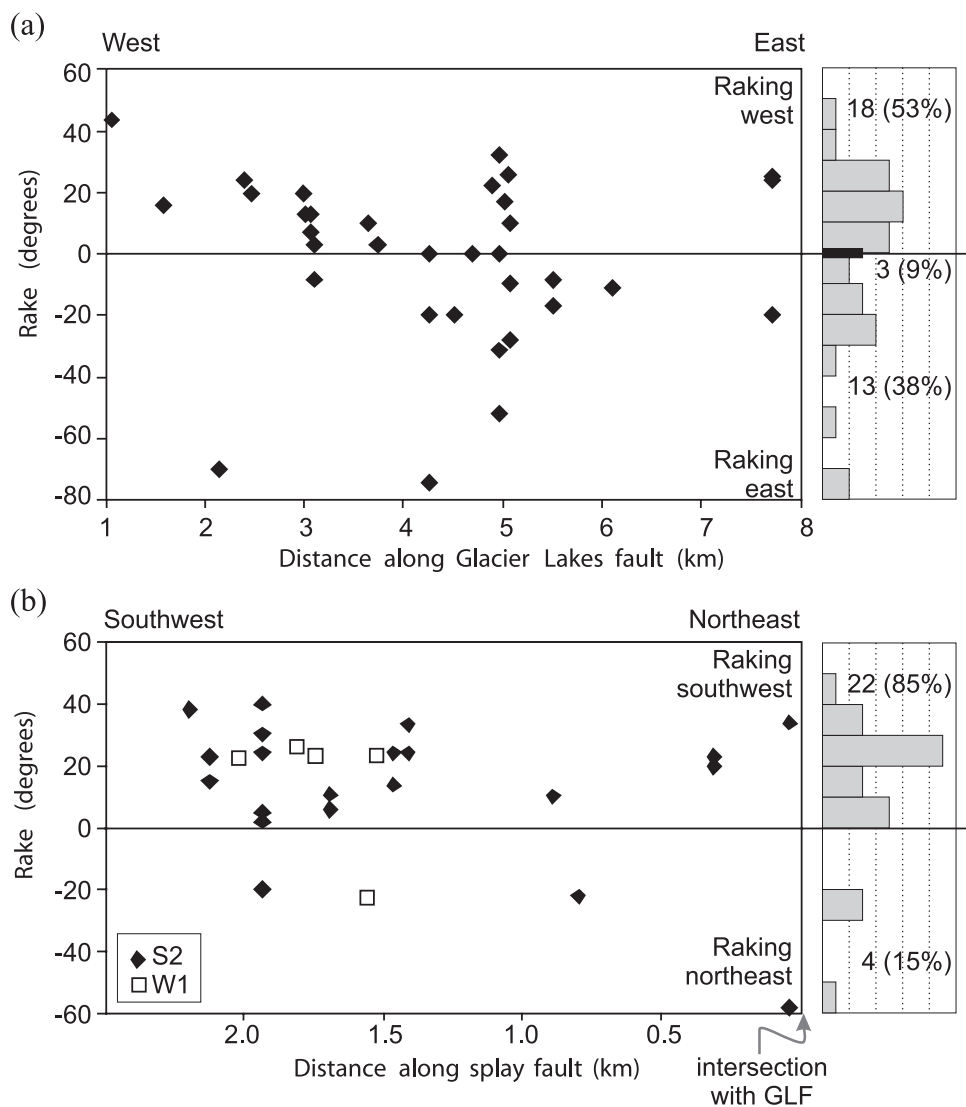
Figure 7. (a) Slickenline rakes versus distance along the Glacier Lakes fault showing approximately equal distribution of east and west raking slickenlines. (b) Slickenline rakes versus distance along S2, one of the splay faults at the termination of the Glacier Lakes fault and along a second splay, W1, linked to S2. The rakes along this splay show a preponderance of oblique slip to the southwest.

fault, accompanied by a broad (~1.4 km wide) zone of secondary faulting in the dilational quadrant of the left-lateral strike-slip GLF. Faults in this region splay from the main fault trace in a counter clockwise sense forming average dihedral angles of 39° with the main fault trace. The splay faults are up to 3 km long, with observed displacements generally decreasing away from the GLF. Similar scale structures are absent in the compressional quadrant of the fault, and also along the GLF farther away from the termination.

[28] The cumulative displacement profile for the GLF alone appears to have a displacement deficit near the tip (Figure 8c). The two most westerly splay faults, closest to the GLF termination, have no data along them (marked in gray on Figure 8a). If the displacement along these faults is modeled as a symmetrical, triangular displacement distribution with a maximum displacement of 15 m, the resulting cumulative displacement distribution approaches that of a smoothly decreasing linear tip profile expected for a single fault [*Cowie and Shipton*, 1998]. The resulting displacement gradient (calculated as the maximum displacement divided by distance from fault tip to the point of maximum displacement) on the GLF is 0.015, well within the range of other measured fault tip displacement gradients. These observations suggest that the splay faults and the GLF are kinematically coherent structures, i.e., displacement is "bleeding off" from the main fault onto the splays at the termination.

[29] Slip vectors defined by slickenlines on slip surfaces are more oblique for the splay faults than for the GLF (Figure 7). A similar relationship has been observed around interacting normal faults, where is it also common to find that the displacement maximum on the intersecting fault is located slightly away from the main fault [e.g., *Maerten et al.*, 1999]. Modeling of intersecting faults by *Maerten et al.*
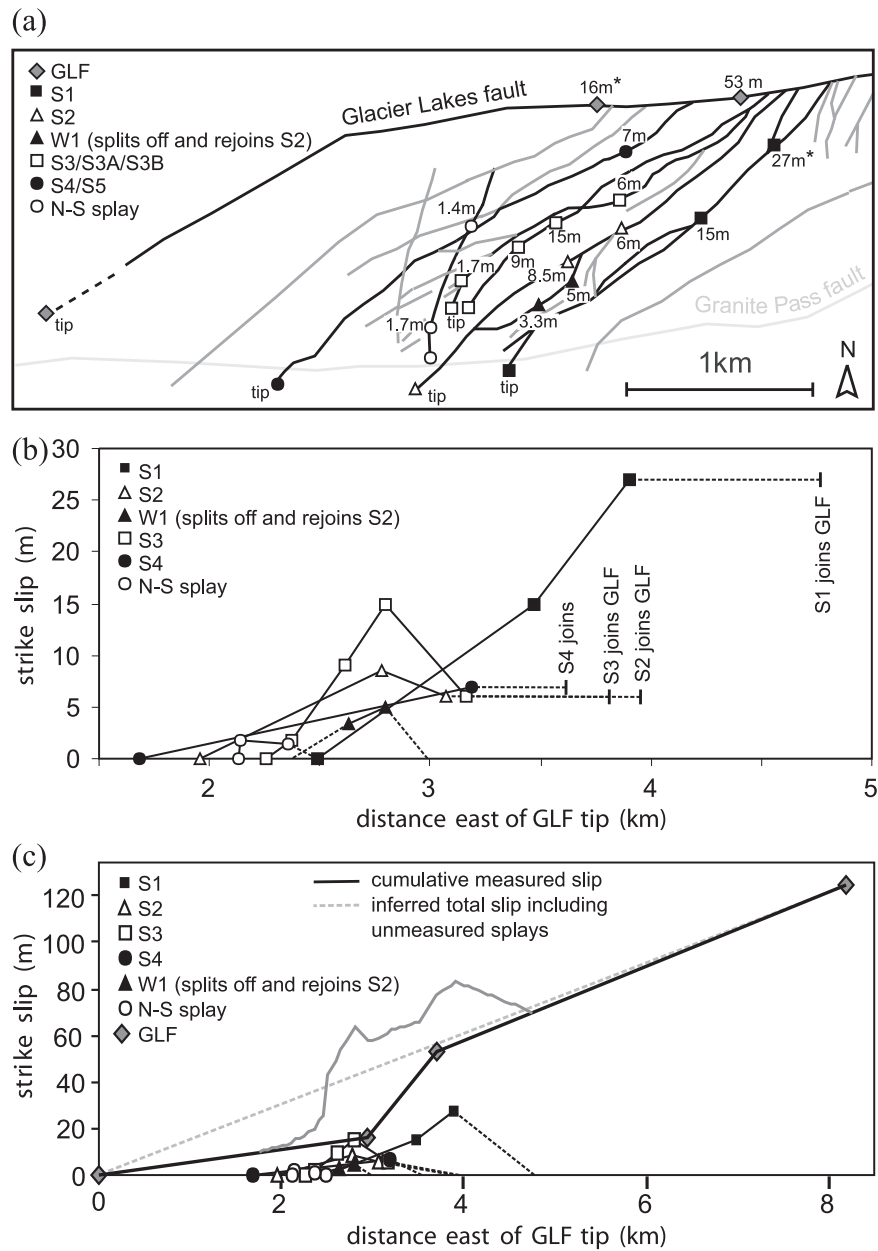
Figure 8. (a) Map of GLF and associated splays showing locations where dike offset and slickenline rake can be used to estimate the amount of strike-slip displacement. Note that the older faults parallel to the GPF have been removed for clarity. Fault strands in gray have no displacement data. Values with stars represent the summed displacement from two fault strands at one location. (b) Displacement profiles for all splays that have two or more displacement data points. Profiles assume linear interpolation between measured displacement values. Dotted lines indicate where each splay intersects the main GLF trace. Displacement assumed to be zero where W1 intersects S2. (c) Profiles for splays and the main GLF. Easternmost displacement estimate from the GLF is from an offset pluton boundary. Note that for all profiles, displacement values have been projected onto an east-west section. The gray curve shows the cumulative measured displacement on the GLF and measured splays assuming that the splays have zero displacement at their intersection with the GLF. If the displacement from splays that have no measurable dike offsets were included (splays in gray in Figure 8a), the cumulative displacement profile would tend to a linear tip displacement profile (gray dotted line).

[2001] suggests that slickenline rakes on the main fault should become more oblique as an intersection is approached. A similar pattern of variable slickenline rakes at segment boundaries was suggested by *Pachell and Evans*

[2002] for the Gemini fault ~55 km to the north of the study area.

[30] Field and microscope observations of ultracataclasites and ductile deformation fabrics within the fault zone
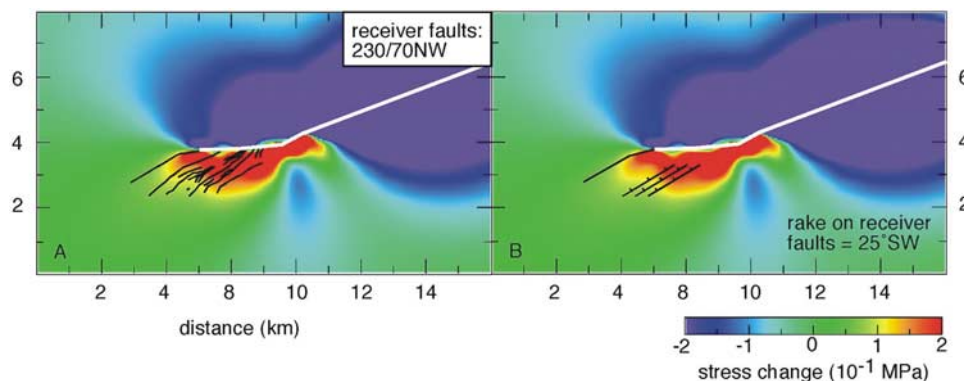
Figure 9. Coulomb failure stress change comparing stress change due to fault slip on the GLF with the distribution of the splay faults. The GLF (white line) is represented as four vertical rectangular dislocations to approximate the bends in the fault trace. From east to west, the four dislocations have 0.4 m, 0.2 m, 0.1 m, and 0.05 m coseismic slip to represent the gradual decrease in displacement shown in Figure 8c. The fault extends from the Earth's surface to 10 km depth and has undergone pure left-lateral slip. We assume that the fault was optimally oriented with respect to the far-field stress; therefore σ_1 plunge is 00 toward 040, σ_2 vertical. Results were sampled at 5 km depth. (a) Distribution of Coulomb failure stress change on hypothetical faults orientated 230/70 NW due to a rupture on the GLF (white line). (b) Three synthetic, frictionless splay faults inserted into the model to test the resolved slip direction. These are rectangular dislocations oriented parallel to the mean splay fault orientation from Figure 5, dipping at 70°, with a top at 2 km and base at 8 km. Tick marks indicate the direction of dip. In the model the splay faults are not physically connected to the GLF. Rakes were measured at nine equally spaced points on each fault surface along the line representing their midpoint (at 5 km depth). Those patches closer to the fault had the same rake as those farther away, though there is likely to be some interaction very close to the fault intersection. The splay faults would be expected to fail with left-lateral slip to the southwest at a rake of 25°.

indicate that the GPF was active at higher pressures and temperatures than the GLF. The GPF and its associated suite of subparallel structures are consistently crosscut by the splay faults from the GLF, but are never observed to crosscut the splays or the GLF. This consistent relation between the two fault systems, together with the absence of ductile fabrics in the GLF boundary faults indicates that the GLF and related splays postdate the GPF. The structure at the western extent of the GLF therefore represents a termination structure, rather than a step over between two coeval strike-slip faults. Although we will not discuss the GPF further, the GPF has been described for the completeness of the data set and because it may have acted as a preexisting structural discontinuity that influenced the GLF development.

[31] The GLF is an exhumed analog for active seismogenic faults, and therefore we use the results of mapping presented here, and petrologic studies underway, to define the composition and structure of a seismogenic fault and gain insight into the processes related to seismic slip at depth. The presence of pseudotachylyte within the fault core material of the GLF is the strongest evidence that the fault slipped at seismic velocities [*Sibson*, 1975; *Magloughlin and Spray*, 1992; *Cowan*, 1999]. As stated earlier if the entire length of the GLF had slipped in a single earthquake, it would have produced an earthquake of magnitude 5.7. An earthquake of this magnitude would be close to the transition between the different scaling regimes for small and large earthquakes (i.e., size regimes 1 and 2 of *Scholz* [2002]). Observations of the termination of the GLF are

therefore significant as the data describe a fault that is at a stage of development either preceding or contemporaneous with this change in scaling relations. The total displacement on the fault is over 100 m; which could not have been accumulated in a single event. The following discussion considers the structure of the GLF termination to be the product of the cumulative displacement on the fault, which was likely accrued by some combination of seismic slip and aseismic creep [*Sibson*, 1989].

[32] The overall geometry of the GLF and splay faults is similar to strike-slip fault terminations observed in many other tectonic settings. Small faults tens of meters long, with displacements up to tens of centimeters often display isolated splay fractures, or arrays of fractures in a horsetail geometry near their tips [*Segall and Pollard*, 1983; *Granier*, 1985; *Martel et al.*, 1988; *Cruikshank et al.*, 1991; *Lim*, 1998]. Such splay fractures develop in the extensional quadrant of small faults, and form similar angles with respect to the main fault trace as the GLF and splay faults. The Gemini fault zone, located in the central Sierra Nevada, is approximately 10 km long with around 100 m displacement, and is composed of a zone of highly fractured and altered host rock bounded by subparallel faults [*Pachell and Evans*, 2002]. The left-lateral Gemini fault zone is interpreted to have evolved from early, joint-nucleated faults and terminates in a series of subsidiary faults that splay counterclockwise from the main fault trace in a similar way to the GLF [*Martel*, 1990; *Pachell and Evans*, 2002]. Analogous structures are observed at the terminations of regional-scale faults tens of kilometers long with hundreds of meters

to kilometers of displacement that likely cut the entire brittle crust [e.g., *Deng et al.*, 1986; *Storti et al.*, 2001; *Micklethwaite and Cox*, 2006] and at mapped surface traces of faults and secondary structures at the terminations of active faults [*DePolo et al.*, 1991; *Vauchez and Da Silva*, 1992; *Bayasgalan et al.*, 1999; *Klinger et al.*, 2005].

5. Coulomb Stress Modeling

[33] The GLF termination structure shows that structural complexity is present at the terminations of faults at depth, as well as around shallow exhumed faults and earthquake ruptures that cut the Earth's surface. Similar deformation should therefore be expected at depth at the end zones of other faults. Models of fault geometry that consider distributed surface complexity tend to focus on a single fault surface at depth are likely to be oversimplified at fault terminations. Linkage zones and step overs between faults, which develop from the interaction of fault terminations [*Martel*, 1990], are therefore also likely to be characterized by distributed deformation at depth.

[34] In order to evaluate whether the splays at the termination of the GLF are consistent with stress changes induced by slip on the main fault, we calculated Coulomb failure stress change for a hypothetical slip event on the GLF using the geometry and kinematics of the GLF from field observations and the method of *King et al.* [1994]. We model a rupture on the GLF approximately equivalent to a M6 earthquake (0.4 m max slip). The distribution of stress changes generated by slip on the GLF resolved onto fault surfaces with the same orientation as the splay faults (taken as 230/70NW) matches well with the distribution of splay faults (Figure 9a). This indicates that we would expect the slip along the splay faults to be triggered by stress changes resulting from a seismic slip event on the GLF.

[35] To test the resolved direction of slip on splay faults that would be triggered by rupture on the main fault we inserted 3 synthetic splay faults and calculated the most likely rake direction that they would fail with. From this calculation splay faults would be expected to fail with left-lateral slip to the southwest at a rake of 25° (Figure 9b). This matches very well with the distribution of rakes measured in the field (Figure 7b). The model results show that the mapped splay fault kinematics are consistent with slip on the splay faults being triggered by slip on the main GLF.

6. Discussion

6.1. Comparison With Model Predictions of Fault Termination Geometries

[36] Several models have been proposed to explain the development of secondary structures at fault tips. Linear elastic fracture mechanics (LEFM) theory predicts that a single secondary fracture will grow at ~70° to the fault plane in response to stress intensification at the tips of a fault [e.g., *Segall and Pollard*, 1980; *Martel*, 1997]. However, geological materials cannot sustain the infinite stresses predicted to occur at fault tips by the LEFM. It is also clear that the field observations of the splay faults at the termination of the GLF cannot be described by LEFM as there

are multiple faults, which form angles of ~39° to the main fault.

[37] Multiple secondary fractures forming angles of <50° with the main fault are predicted by models of quasi-static fault growth that incorporate a cohesive zone ahead of the fault tip in which shear stress is elevated [*Cooke*, 1997; *Martel*, 1997]. Although at least some of the displacement on the GLF was seismogenic, quasi-static processes may predominate during interseismic periods [*Sibson*, 1989]. *Cooke* [1997] showed that development of more than one splay fault is promoted by a spatial variation of frictional strength in the end zone of the fault, which would also result in a steep displacement gradient as the displacement on the fault tends to zero. The displacement gradient at the tip of the GLF is 0.015 (Figure 8c), a similar order of magnitude to gradients observed at other fault tips [*Shipton and Cowie*, 2001]. *Bürgmann et al.* [1994] suggested that other factors that may control displacement gradients include an inhomogeneous stress field due to fault interaction, inelastic deformation in the tip region of faults, and spatially variable host rock elastic modulus. From our mapping we suggest that inelastic deformation at the fault tip, in the form of splay faults, causes the GLF displacement gradient to remain low near the fault termination (Figure 8). The GLF and splays cut across several preexisting fault zones (the GPF and subparallel faults). Interaction with these faults, which will have distinct elastic properties from the host rock, may have influenced the development of multiple splays at the termination of the GLF.

[38] Recent two-dimensional (2-D) [*Yamashita*, 2000; *Poliakov et al.*, 2002; *Andrews*, 2005; *Rice et al.*, 2005] and 3-D [*Aochi and Fukuyama*, 2002; *Dalguer et al.*, 2003] models of dynamic rupture propagation show that the stress changes induced by a dynamic shear rupture process are sufficient to generate secondary structures in a volume surrounding a fault plane (Figure 10). All of these models predict that the majority of the deformation develops in the dilational quadrant at the rupture tip. In the 2-D models of *Andrews* [2005] the width of the zone of off-fault deformation increases as the dynamic rupture propagates, resulting in a triangular zone of off-fault deformation in the dilational quadrant. However, in the 3-D models of *Dalguer et al.* [2003] the width varies as a complex function of the primary fault geometry. Off-fault deformation is also dependent upon rupture speed, stress drop, static and dynamic friction coefficients, and other rupture properties [*Poliakov et al.*, 2002; *Rice et al.*, 2005].

[39] The steeply dipping GLF is exposed in a plane oriented approximately perpendicular to the fault and which contains the slip vector (i.e., a horizontal plane of exposure for a pure strike-slip fault). Assuming that the plane of exposure cuts the fault midway through the fault width allows the mapped geometry of the GLF to be compared with results of dynamic rupture models. Comparisons between the field observations and the model predictions in this case are valid if an earthquake rupture had ruptured the entire length of the GLF (i.e., the rupture did not stop partway along the fault). However, it is likely that the fault accommodated a variety of earthquake sizes, possibly following a Gutenberg-Richter distribution. If the fault mainly slipped in smaller earthquakes, we might expect to
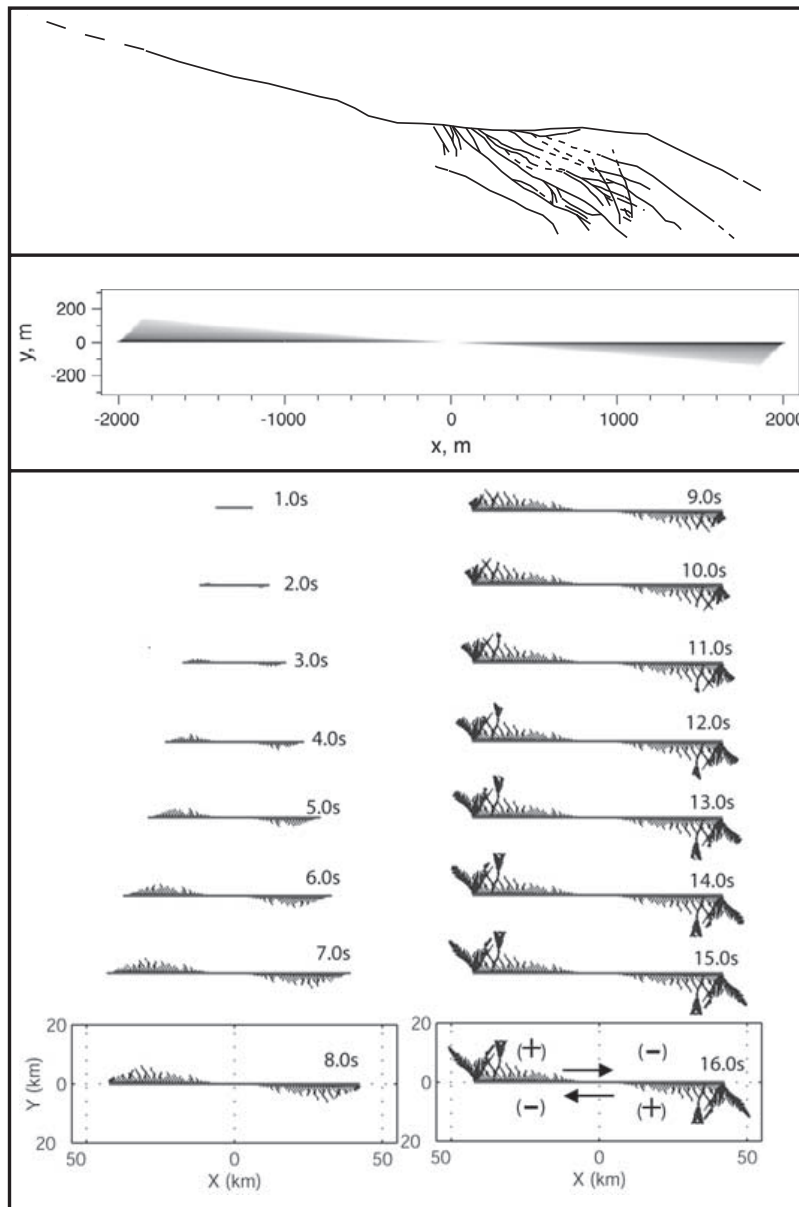
Figure 10. Comparison of the geometry of the GLF termination (top, plot has been inverted to allow comparison of the left-lateral GLF with the right-lateral model faults) with the model predictions of (middle) *Andrews* [2005] and (bottom) *Dalguer et al.* [2003, p. 5]. In each case, off-fault damage is present in the dilational quadrant of the fault, with GLF splay fault orientations matching the orientations of new cracks developed under the model conditions of *Dalguer et al.* [2003].

see the damage zone reflecting the distribution of earthquake sizes. Our mapping shows that subsidiary structures are only developed at the western termination of the GLF, suggesting that a potentially large population of small earthquakes made little impact on the damage distribution.

[40] The geometry of the termination is an asymmetrical zone of damage emanating from the GLF into the dilational quadrant, similar to the models (Figure 10). Within the zone of damage the greatest intensity of strain (highest measured strike slip values on the splay faults) is located adjacent to the GLF fault plane (Figure 8), similar to the results of *Andrews* [2005]. The ratio between the width of the zone of splays and the minimum fault length (≤0.170) is also

similar to the value of ∼0.075 predicted by *Andrews* [2005], and would be the same if the GLF was 18.6 km long. The GLF splays are oriented at a counterclockwise acute angle to the main fault as in the model of *Dalguer et al.* [2003]. However, the wedge-shaped zone of off-fault deformation expected from several models is less well matched by the field observations (see Figure 10). The calculated Coulomb failure stress changes for a slip event on the GLF (Figure 9) suggest that bends in the fault trace may be partly responsible for this discrepancy.

[41] The geometry of the GLF termination structure seems to approximate the off-fault damage geometries predicted by both the quasi-static and dynamic models of

fault growth. At the scale of the data presented in this paper (kilometer-scale), there are no geometrical features predicted by either of the two sets of models that would allow the process of formation to be distinguished. Ancient seismic activity has been demonstrated for the GLF from the presence of pseudotachylytes, suggesting that dynamically induced off-fault damage should be expected. However, quasi-static processes may have been prevalent during interseismic periods. It is therefore probable that the off-fault damage present around the GLF represents the superimposition of interseismic and coseismic processes. A future line of research could be to investigate the potential presence or absence of structures in the fault damage zone that are indicative of dynamic slip events; high angle secondary fractures [*Di Toro et al.*, 2005], or fractures with a branching morphology [*Sagy et al.*, 2001; *Kame and Yamashita*, 2003] have been suggested to develop only under dynamic stress.

6.2. Implications for Rupture Propagation

[42] Models of rupture propagation [*Harris and Day*, 1999; *Kase and Kuge*, 2001] often assume that a slip patch or shear rupture propagates along a fault that is hosted in undeformed rock. However, the field data presented in this paper indicate that fault terminations at seismogenic depths are not contained within intact rock, and that the secondary structures associated with terminations take the form of macroscale faulting, as well as likely microfracturing [*Vermilye and Scholz*, 1998]. Fracturing of a host rock in this manner will change the bulk elastic properties of the rock [*Walsh*, 1965; *O'Connell and Budiansky*, 1974; *Ayling et al.*, 1995; *Ciccotti and Mulargia*, 2004; *Faulkner et al.*, 2006; *Nasseri et al.*, 2007;], and lead to interaction between the secondary fractures and a dynamically propagating rupture front that will complicate the rupture growth [*Yamashita*, 2000; *Andrews*, 2005]. The effects of preexisting deformation on rupture processes must therefore be considered.

[43] It is unlikely that the structures present in the end zone of the GLF were produced entirely by the most recent earthquake rupture as they have very large total displacement with respect to the magnitude of observed coseismic slip. Earthquake ruptures occurring on the GLF must have interacted with the splay faults at the fault termination. Displacement on splay faults at the GLF termination was therefore accumulated over a significant fraction of the fault's history. This conclusion is reasonable as the majority of fault growth models that are derived from field observations [e.g., *Chester and Logan*, 1986; *Martel*, 1990; *Mansfield and Cartwright*, 1996; *Seront et al.*, 1998] predict that a zone of damaged rock evolves around a fault as a fault accumulates displacement. By the time a fault has grown to a size that would generate intermediate to large earthquakes, the rock surrounding the fault plane will contain numerous opening mode and shear fractures that will act as planes of preferential weakness. Such subsidiary structures will also induce a heterogeneous spatial distribution of elastic properties. *Willson et al.* [2007] model cracks propagating through host rock with heterogeneous material properties and show that the locations and frequencies of evolving splay fractures are heavily influenced by the spatial distribution of such heterogeneities.

[44] Models that examine the potential for ruptures to propagate beyond fault ends, or through step overs between two faults [*Harris and Day*, 1999; *Kase and Kuge*, 2001] are directly investigating the zones where secondary structures are likely to be present. The effect of secondary macroscale and microscale fracturing is to lower the elastic moduli of the medium in which they are contained [*Walsh*, 1965]. The presence of preexisting structures at fault terminations will therefore reduce the elastic moduli in those regions. *Rice and Cocco* [2007] suggest that understanding the high strain rate constitutive response of the damage zone to dynamic slip is crucial to understanding the interaction between slip on a fault and its off-fault damage zone. They add that a nonlinear response off the fault plane may alter the normal stress on the fault itself [see also *Faulkner et al.*, 2006] and affect the energy balance of an earthquake rupture. A similar distribution of subsidiary structures would also be predicted at other discontinuities such as step overs. Defining the extent and nature of the secondary structures around faults is therefore crucial to allow the effects of the damaged rock to be accounted for in models of rupture propagation.

6.3. Structural Controls on Aftershock Distribution

[45] The splay faults present in the end zone of the GLF are up to 3 km long and so could have experienced earthquakes up to magnitude $M_w \sim 5.1$ if the entire mapped length of the splays had slipped [*Wells and Coppersmith*, 1994]. This magnitude is a similar size to observed aftershocks following magnitude $M_w \sim 5.7$ main shocks, the maximum magnitude of an earthquake that would rupture the entire length of the GLF [e.g., *Scholz*, 2002]. Areas of positive changes in Coulomb failure stress have been shown to correlate with the distribution of aftershocks around main shock ruptures [*King et al.*, 1994; *Toda et al.*, 1998; *Freed*, 2005]. Figure 9a therefore suggests that shear displacement on the splays could have accumulated during aftershock activity to a rupture on the main GLF fault plane. The splay faults at the GLF termination are approximately planar structures with a narrow range of orientations (see Figure 5), so aftershocks nucleating on the splays would have a limited range of possible focal mechanisms. Slip vectors measured from slickenlines exposed on the splay faults show more oblique rakes than the main fault (Figure 7), also consistent with static stress transfer modeling (Figure 9b). The field data and model results would predict that any aftershocks should also have oblique slip vectors. This field data suggests a strong structural control on the distribution and focal mechanism of aftershocks when a rupture end coincides with a fault termination.

[46] *Hardebeck* [2006] showed that the focal mechanisms of closely spaced aftershocks of the 1989 Loma Prieta earthquake were very similar on scales of 0.5–5 km. At larger scales the aftershock focal mechanisms became increasingly heterogeneous, leading to the conclusion that that the homogeneity of the small-scale aftershock focal mechanisms was due to faults of similar orientations slipping in each aftershock. *Collettini and Trippetta* [2007] suggest that in typical continental crust there is a wide range of fault orientations that could slip during an earthquake, but that only the faults optimally oriented for slip will be triggered to form aftershocks. However, if a systematic

distribution of secondary structures is present around the main fault, as is the case for the GLF, then it seems likely that the orientations of the secondary structures would control the aftershock focal mechanisms, rather than just the orientation of the regional (effective) stress field. We would therefore predict a narrow range of aftershock focal mechanisms determined by the preexisting fault termination structures.

7. Conclusions

[47] 1. The left-lateral Glacier Lakes fault, Sierra Nevada, California, has been exhumed from ~6–8 km depth. Field observations show that the western termination of the fault is defined by a series of splay faults, up to 3 km long, forming dihedral angles of $13–60°$ with the main fault trace, that extend into the dilational quadrant of the fault.

[48] 2. Pseudotachylytes identified within the fault core of the GLF indicate that the fault was, at least in part, seismically active.

[49] 3. The geometry of the GLF termination is similar to those of other exhumed faults in the Sierra Nevada and elsewhere, and to the terminations of earthquake ruptures observed at the Earth's surface.

[50] 4. Field observations of the exhumed GLF demonstrate that the complexity observed in association with the terminations of fault traces at the surface can also be expected at seismogenic depths.

[51] 5. Splay fault geometry at the tip of the GLF is well predicted by quasi-static models of fault growth. The zone of deformation at the fault tip defined by the splays also appears to match the predictions of off-fault damage associated with dynamic rupture propagation.

[52] 6. The elastic properties of host rocks are different at fault terminations and step overs due to the accumulation of damage structures in these regions, and must be accounted for in models of dynamic rupture propagation beyond fault terminations, or across other structural discontinuities.

[53] 7. Aftershock distributions and focal mechanisms may be controlled by the size, geometry and kinematics of structures present at fault terminations.

References

Ague, J. J., and G. H. Brimhall (1988), Magmatic arc asymmetry and distribution of anomalous plutonic belts in the batholiths of California—Effects of assimilation, crustal thickness, and depth of crystallization, *Geol. Soc. Am. Bull.*, *100*, 912–927, doi:10.1130/0016-7606(1988) 100<0912:MAAADO>2.3.CO;2.

Aki, K. (1979), Characterization of barriers on an earthquake fault, *J. Geophys. Res.*, *84*, 6140–6148, doi:10.1029/JB084iB11p06140.

Andrews, D. J. (2005), Rupture dynamics with energy loss outside the slip zone, *J. Geophys. Res.*, *110*, B01307, doi:10.1029/2004JB003191.

Aochi, H., and E. Fukuyama (2002), Three-dimensional nonplanar simulation of the 1992 Landers earthquake, *J. Geophys. Res.*, *107*(B2), 2035, doi:10.1029/2000JB000061.

Aydin, A., and Y. J. Du (1995), Surface rupture at a fault bend—The 28-June-1992 Landers, California, earthquake, *Bull. Seismol. Soc. Am.*, *85*, 111–128.

Ayling, M. R., P. G. Meredith, and S. A. F. Murrell (1995), Microcracking during triaxial deformation of porous rocks monitored by changes in rock physical-properties. 1. Elastic-wave propagation measurements on dry rocks, *Tectonophysics*, *245*, 205–221, doi:10.1016/0040-1951(94)00235-2.

Barka, A. (1996), Slip distribution along the north Anatolian fault associated with the large earthquakes of the period 1939 to 1967, *Bull. Seismol. Soc. Am.*, *86*, 1238–1254.

Bateman, P. C. (1992), Plutonism in the central part of the Sierra Nevada Batholith, California, *U.S. Geol. Surv. Prof. Pap.*, *1483*, 186 pp.

Bayasgalan, A., J. Jackson, J. F. Ritz, and S. Carretier (1999), Field examples of strike-slip fault terminations in Mongolia and their tectonic significance, *Tectonics*, *18*, 394–411, doi:10.1029/1999TC900007.

Berger, G. W., and D. York (1981), Geothermometry from $^{40}Ar-^{39}Ar$ dating experiments, *Geochim. Cosmochim. Acta*, *45*, 795–811, doi:10.1016/0016-7037(81)90109-5.

Bürgmann, R., D. D. Pollard, and S. J. Martel (1994), Slip distributions on faults—Effects of stress gradients, inelastic deformation, heterogeneous host-rock stiffness, and fault interaction, *J. Struct. Geol.*, *16*, 1675–1690, doi:10.1016/0191-8141(94)90134-1.

Chester, F. M., and J. M. Logan (1986), Implications for mechanical-properties of brittle faults from observations of the Punchbowl Fault Zone, California, *Pure Appl. Geophys.*, *124*, 79–106, doi:10.1007/BF00875720.

Christiansen, P. P., and D. D. Pollard (1997), Nucleation, growth and structural development of mylonitic shear zones in granitic rock, *J. Struct. Geol.*, *19*, 1159–1172, doi:10.1016/S0191-8141(97)00025-4.

Ciccotti, M., and E. Mulargia (2004), Differences between static and dynamic elastic moduli of a typical seismogenic rock, *Geophys. J. Int.*, *157*, 474–477, doi:10.1111/j.1365-246X.2004.02213.x.

Collettini, C., and F. Trippetta (2007), A slip tendency analysis to test mechanical and structural control on aftershock rupture planes, *Earth Planet. Sci. Lett.*, *255*, 402–413, doi:10.1016/j.epsl.2007.01.001.

Cooke, M. L. (1997), Fracture localization along faults with spatially varying friction, *J. Geophys. Res.*, *102*, 22,425–22,434, doi:10.1029/97JB01829.

Cowan, D. S. (1999), Do faults preserve a record of seismic slip? A field geologist's opinion, *J. Struct. Geol.*, *21*, 995–1001, doi:10.1016/S0191-8141(99)00046-2.

Cowie, P. A., and Z. K. Shipton (1998), Fault tip displacement gradients and process zone dimensions, *J. Struct. Geol.*, *20*, 983–997, doi:10.1016/S0191-8141(98)00029-7.

Cruikshank, K. M., G. H. Zhao, and A. M. Johnson (1991), Analysis of minor fracture associated with joints and faulted joints, *J. Struct. Geol.*, *13*, 865–886, doi:10.1016/0191-8141(91)90083-U.

Curewitz, D., and J. A. Karson (1997), Structural settings of hydrothermal outflow: Fracture permeability maintained by fault propagation and interaction, *J. Volcanol. Geotherm. Res.*, *79*, 149–168, doi:10.1016/S0377-0273(97)00027-9.

d'Alessio, M., and S. J. Martel (2005), Development of strike-slip faults from dikes, Sequoia National Park, California, *J. Struct. Geol.*, *27*, 35–49, doi:10.1016/j.jsg.2004.06.013.

Dalguer, L. A., K. Irikura, and J. D. Riera (2003), Simulation of tensile crack generation by three-dimensional dynamic shear rupture propagation during an earthquake, *J. Geophys. Res.*, *108*(B3), 2144, doi:10.1029/2001JB001734.

Deng, Q. D., D. N. Wu, P. Z. Zhang, and S. F. Chen (1986), Structure and deformational character of strike-slip-fault zones, *Pure Appl. Geophys.*, *124*, 203–223, doi:10.1007/BF00875726.

DePolo, C. M., D. G. Clark, D. B. Slemmons, and A. R. Ramelli (1991), Historical surface faulting in the Basin and Range Province, western North-America—Implications for fault segmentation, *J. Struct. Geol.*, *13*, 123–136, doi:10.1016/0191-8141(91)90061-M.

Di Toro, G., S. Nielsen, and G. Pennacchioni (2005), Earthquake rupture dynamics frozen in exhumed ancient faults, *Nature*, *436*, 1009–1012, doi:10.1038/nature03910.

Dodge, G. C. W., and J. G. Moore (1968), Occurrence and composition of biotites from the Cartridge Pass pluton of the Sierra Nevada batholith, California, *U.S. Geol. Surv. Prof. Pap.*, *600-B*, 6–10.

Evans, J. P., Z. K. Shipton, M. A. Pachell, S. J. Lim, and K. R. Robeson (2000), The structure and composition of exhumed faults, and their implications for seismic processes, paper presented at the 3rd Conference on the Tectonic Problems of the San Andreas Fault System, Stanford Univ., Stanford, Calif.

Evernden, J. F., and R. W. Kistler (1970), Chronology of emplacement of Mesozoic batholithic complexes in California and western Nevada, *U. S. Geol. Surv. Prof. Pap.*, 632, 42 pp.

Faulkner, D. R., T. M. Mitchell, D. Healy, and M. J. Heap (2006), Slip on 'weak' faults by the rotation of regional stress in the fracture damage zone, *Nature*, 444, 922–925, doi:10.1038/nature05353.

Freed, A. M. (2005), Earthquake triggering by static, dynamic, and post-seismic stress transfer, *Annu. Rev. Earth Planet. Sci.*, 33, 335–367, doi:10.1146/annurev.earth.33.092203.122505.

Granier, T. (1985), Origin, damping and pattern of faults in granite, *Tectonics*, 4, 721–737, doi:10.1029/TC004i007p00721.

Hardebeck, J. L. (2006), Homogeneity of small-scale earthquake faulting, stress, and fault strength, *Bull. Seismol. Soc. Am.*, 96, 1675–1688, doi:10.1785/0120050257.

Harris, R. A., and S. M. Day (1999), Dynamic 3D simulations of earthquakes on en echelon faults, *Geophys. Res. Lett.*, 26, 2089–2092, doi:10.1029/1999GL900377.

House, M. A., B. P. Wernicke, and K. A. Farley (1998), Dating topography of the Sierra Nevada, California, using apatite (U-Th)/He ages, *Nature*, 396, 66–69, doi:10.1038/23926.

Kame, N., and T. Yamashita (2003), Dynamic branching, arresting of rupture and the seismic wave radiation in self-chosen crack path modelling, *Geophys. J. Int.*, 155, 1042–1050, doi:10.1111/j.1365-246X.2003.02113.x.

Kase, Y., and K. Kuge (2001), Rupture propagation beyond fault discontinuities: significance of fault strike and location, *Geophys. J. Int.*, 147, 330–342, doi:10.1046/j.1365-246X.2001.00533.x.

Kim, Y. S., and D. J. Sanderson (2006), Structural similarity and variety at the tips in a wide range of strike-slip faults: a review, *Terra Nova*, 18, 330–344.

King, G., and J. Nabelek (1985), Role of fault bends in the initiation and termination of earthquake rupture, *Science*, 228, 984–987, doi:10.1126/science.228.4702.984.

King, G. C. P., R. S. Stein, and J. Lin (1994), Static stress changes and the triggering of earthquakes, *Bull. Seismol. Soc. Am.*, 84, 935–953.

Klinger, Y., X. W. Xu, P. Tapponnier, J. Van der Woerd, C. Lasserre, and G. King (2005), High-resolution satellite imagery mapping of the surface rupture and slip distribution of the MW similar to 7.8, 14 November 2001 Kokoxili earthquake, Kunlun Fault, northern Tibet, China, *Bull. Seismol. Soc. Am.*, 95, 1970–1987, doi:10.1785/0120040233.

Lim, S. J. (1998), Small strike-slip faults in granitic rock: implications for three-dimensional models, M.S. thesis, Utah State Univ., Logan.

Maerten, L., E. J. M. Willemse, D. D. Pollard, and K. Rawnsley (1999), Slip distributions on intersecting normal faults, *J. Struct. Geol.*, 21, 259–271, doi:10.1016/S0191-8141(98)00122-9.

Maerten, L., D. D. Pollard, and F. Maerten (2001), Digital mapping of three-dimensional structures of the Chimney Rock fault system, central Utah, *J. Struct. Geol.*, 23, 585–592, doi:10.1016/S0191-8141(00)00142-5.

Magloughlin, J. F., and J. G. Spray (1992), Frictional melting processes and products in geological-materials—Introduction and discussion, *Tectonophysics*, 204, 197–206, doi:10.1016/0040-1951(92)90307-R.

Mansfield, C. S., and J. A. Cartwright (1996), High resolution fault displacement mapping from three-dimensional seismic data: Evidence for dip linkage during fault growth, *J. Struct. Geol.*, 18, 249–263, doi:10.1016/S0191-8141(96)80048-4.

Martel, S. J. (1990), Formation of compound strike-slip-fault zones, Mount Abbot Quadrangle, California, *J. Struct. Geol.*, 12, 869–882, doi:10.1016/0191-8141(90)90060-C.

Martel, S. J. (1997), Effects of cohesive zones on small faults and implications for secondary fracturing and fault trace geometry, *J. Struct. Geol.*, 19, 835–847, doi:10.1016/S0191-8141(97)00002-3.

Martel, S. J., and W. A. Boger (1998), Geometry and mechanics of secondary fracturing around small three-dimensional faults in granitic rock, *J. Geophys. Res.*, 103, 21,299–21,314, doi:10.1029/98JB01393.

Martel, S. J., D. D. Pollard, and P. Segall (1988), Development of simple strike-slip-fault zones, Mount Abbot Quadrangle, Sierra-Nevada, California, *Geol. Soc. Am. Bull.*, 100, 1451–1465, doi:10.1130/0016-7606(1988)100<1451:DOSSSF>2.3.CO;2.

McGrath, A. G., and I. Davison (1995), damage zone geometry around fault tips, *J. Struct. Geol.*, 17, 1011–1024, doi:10.1016/0191-8141(94)00116-H.

Micklethwaite, S., and S. F. Cox (2004), Fault-segment rupture, aftershock-zone fluid flow, and mineralization, *Geology*, 32, 813–816, doi:10.1130/G20559.1.

Micklethwaite, S., and S. F. Cox (2006), Progressive fault triggering and fluid flow in aftershock domains: Examples from mineralized Archaean fault systems, *Earth Planet. Sci. Lett.*, 250, 318–330, doi:10.1016/j.epsl.2006.07.050.

Moore, J. G. (1978), Geologic map of the Marion Peak Quadrangle, Fresno County, geologic quadrangle map, U.S. Geol. Surv., Menlo Park, Calif.

Nasseri, M. H. B., A. Schubnel, and R. P. Young (2007), Coupled evolutions of fracture toughness and elastic wave velocities at high crack density in thermally treated Westerly granite, *Int. J. Rock Mech. Mineral. Sci.*, 44, 601–616, doi:10.1016/j.ijrmms.2006.09.008.

Noyes, H. J., D. R. Wones, and F. A. Frey (1983), A tale of 2 plutons—Petrographic and mineralogic constraints on the petrogenesis of the Red Lake and Eagle Peak plutons, central Sierra-Nevada, California, *J. Geol.*, 91, 353–379.

O'Connell, R. J., and B. Budiansky (1974), Seismic velocities in dry and saturated cracked solids, *J. Geophys. Res.*, 79, 5412–5426, doi:10.1029/JB079i035p05412.

Pachell, M. A., and J. P. Evans (2002), Growth, linkage, and termination processes of a 10-km-long strike-slip fault in jointed granite: the Gemini fault zone, Sierra Nevada, California, *J. Struct. Geol.*, 24, 1903–1924, doi:10.1016/S0191-8141(02)00027-5.

Poliakov, A. N. B., R. Dmowska, and J. R. Rice (2002), Dynamic shear rupture interactions with fault bends and off-axis secondary faulting, *J. Geophys. Res.*, 107(B11), 2295, doi:10.1029/2001JB000572.

Rice, J. R., and M. Cocco (2007), Seismic fault rheology and earthquake dynamics, in *Tectonic Faults: Agents of Change on a Dynamic Earth*, edited by M. R. Handy et al., pp. 99–138, Mass. Inst. of Technol., Cambridge.

Rice, J. R., C. G. Sammis, and R. Parsons (2005), Off-fault secondary failure induced by a dynamic slip pulse, *Bull. Seismol. Soc. Am.*, 95, 109–134, doi:10.1785/0120030166.

Sagy, A., Z. Reches, and I. Roman (2001), Dynamic fracturing: field and experimental observations, *J. Struct. Geol.*, 23, 1223–1239, doi:10.1016/S0191-8141(00)00190-5.

Scholz, C. H. (2002), *The Mechanics of Earthquakes and Faulting*, Cambridge Univ. Press, New York.

Segall, P., and D. D. Pollard (1980), Mechanics of discontinuous faults, *J. Geophys. Res.*, 85, 4337–4350, doi:10.1029/JB085iB08p04337.

Segall, P., and D. D. Pollard (1983), Nucleation and growth of strike-slip faults in granite, *J. Geophys. Res.*, 88, 555–568, doi:10.1029/JB088iB01p00555.

Segall, P., E. H. McKee, S. J. Martel, and B. D. Turrin (1990), Late Cretaceous age of fractures in the Sierra-Nevada Batholith, California, *Geology*, 18, 1248–1251, doi:10.1130/0091-7613(1990)018<1248:LCAOFI>2.3.CO;2.

Seront, B., T. F. Wong, J. S. Caine, C. B. Forster, R. L. Bruhn, and J. T. Fredrich (1998), Laboratory characterization of hydromechanical properties of a seismogenic normal fault system, *J. Struct. Geol.*, 20, 865–881, doi:10.1016/S0191-8141(98)00023-6.

Shipton, Z. K., and P. A. Cowie (2001), Damage zone and slip-surface evolution over mu m to km scales in high-porosity Navajo sandstone, Utah, *J. Struct. Geol.*, 23, 1825–1844, doi:10.1016/S0191-8141(01)00059-9.

Sibson, R. H. (1975), Generation of pseudotachylyte by ancient seismic faulting, *Geophys. J. R. Astron. Soc.*, 43, 775–794.

Sibson, R. H. (1985), Stopping of earthquake ruptures at dilational fault jogs, *Nature*, 316, 248–251, doi:10.1038/316248a0.

Sibson, R. H. (1987), Earthquake rupturing as a mineralizing agent in hydrothermal systems, *Geology*, 15, 701–704, doi:10.1130/0091-7613(1987)15<701:ERAAMA>2.0.CO;2.

Sibson, R. H. (1989), Earthquake faulting as a structural process, *J. Struct. Geol.*, 11, 1–14, doi:10.1016/0191-8141(89)90032-1.

Storti, F., F. Rossetti, and F. Salvini (2001), Structural architecture and displacement accommodation mechanisms at the termination of the Priestley Fault, northern Victoria Land, Antarctica, *Tectonophysics*, 341, 141–161, doi:10.1016/S0040-1951(01)00198-6.

Tikoff, B., and M. de Saint Blanquat (1997), Transpressional shearing and strike-slip partitioning in the Late Cretaceous Sierra Nevada magmatic arc, California, *Tectonics*, 16, 442–459, doi:10.1029/97TC00720.

Tobisch, O. T., and A. R. Cruden (1995), Fracture-controlled magma conduits in an obliquely convergent continental magmatic arc, *Geology*, 23, 941–944, doi:10.1130/0091-7613(1995)023<0941:FCMCIA>2.3.CO;2.

Toda, S., R. S. Stein, P. A. Reasenberg, J. H. Dieterich, and A. Yoshida (1998), Stress transferred by the 1995 M_w = 6.9 Kobe, Japan, shock: Effect on aftershocks and future earthquake probabilities, *J. Geophys. Res.*, 103, 24,543–24,565, doi:10.1029/98JB00765.

Vauchez, A., and M. E. Da Silva (1992), Termination of a continental-scale strike-slip-fault in partially melted crust—The West Pernambuco Shear Zone, northeast Brazil, *Geology*, 20, 1007–1010, doi:10.1130/0091-7613(1992)020<1007:TOACSS>2.3.CO;2.

Vermilye, J. M., and C. H. Scholz (1998), The process zone: A microstructural view of fault growth, *J. Geophys. Res.*, 103, 12,223–12,237, doi:10.1029/98JB00957.

Walsh, J. B. (1965), Effect of cracks on uniaxial elastic compression of rocks, *J. Geophys. Res.*, 70, 381–389, doi:10.1029/JZ070i002p00381.

Wells, D. L., and K. J. Coppersmith (1994), New empirical relationships among magnitude, rupture length, rupture width, rupture area, and surface displacement, *Bull. Seismol. Soc. Am.*, *84*, 974–1002.

Wesnousky, S. G. (2006), Predicting the endpoints of earthquake ruptures, *Nature*, *444*, 358–360, doi:10.1038/nature05275.

Willson, J. P., R. J. Lunn, and Z. K. Shipton (2007), Simulating spatial and temporal evolution of multiple wing cracks around faults in crystalline basement rocks, *J. Geophys. Res.*, *112*, B08408, doi:10.1029/2006JB004815.

Yamashita, T. (2000), Generation of microcracks by dynamic shear rupture and its effects on rupture growth and elastic wave radiation, *Geophys. J. Int.*, *143*, 395–406, doi:10.1046/j.1365-246X.2000.01238.x.

_____

J. P. Evans and S. J. Lim, Department of Geology, Utah State University, Logan, UT 84322-4505, USA.

J. D. Kirkpatrick and Z. K. Shipton, Department of Geographical and Earth Sciences, University of Glasgow, Glasgow G12 8QC, UK. (james.kirkpatrick@ges.gla.ac.uk)

S. Micklethwaite, Research School of Earth Sciences, Australian National University, Canberra ACT 0200, Australia.